Explicit consideration of near-fault directivity effects and treatment of distributed seismicity as finite-faults in NZ-specific probabilistic seismic hazard analysis

V.A. Joshi, B.A. Bradley

University of Canterbury, Christchurch, New Zealand.

2014 NZSEE Conference

ABSTRACT: This paper concerns the explicit consideration of near-fault directivity in conventional ground motion prediction models, and its implication for probabilistic seismic hazard analysis (PSHA) in New Zealand. The proposed approach utilises recently developed models by Shahi & Baker (2011), which account for both the 'narrowband' nature of the directivity pulse on spectral ordinates, and the probability of pulse occurrence at the site of interest. Furthermore, in order to correctly consider directivity, distributed seismicity sources are considered as finite-faults, as opposed to their (incorrect) conventional treatment as point-sources. The significance of directivity on hazard analysis results is illustrated for various vibration periods at generic sites located in Christchurch and Otira, two locations whose seismic hazard is comprised of notably different seismic sources. When compared to the PSHA results considering directivity and distributed seismicity as finite faults, it is shown that the NZS1170.5:2004 directivity factor is notably unconservative for all vibration periods in Otira (i.e. high seismic hazard region); and unconservative for Christchurch at short-to-moderate vibration periods (T < 3s); but conservative at long periods (T > 4s).

1 INTRODUCTION

Forward-directivity is a physical phenomenon which can potentially produce damaging pulse-like ground motions in the near-fault region. The pulse-like feature in these ground motions is typically observed at the beginning of the fault-normal velocity time-series, and is caused by the alignment of rupture front and slip direction along the causative fault towards a given site (Somerville et al., 1997). The tremendous damage potential of the directivity phenomenon has been observed in major worldwide earthquakes such as the 1971 San Fernando, 1994 Northridge and 1995 Kobe events. The 2010-2011 Canterbury earthquake sequence produced severe ground motions which were well-recorded by a dense array of high quality instrumentation in Christchurch and the surrounding Canterbury Plains. Recent studies (Bradley & Cubrinovski, 2011; Bradley, 2012b; Joshi & Bradley, 2013) have clearly identified the presence of forward-directivity effects in near-fault ground motions resulting from the 4 September 2010 M_w7.1 Darfield and 22 February 2011 M_w6.2 Christchurch earthquakes.

Figure 1 illustrates the observed velocity time-series and elastic pseudo-acceleration response spectrum corresponding to the ground motion recorded at Lincoln (LINC) during the M_w7.1 Darfield earthquake. Evidence of forward-directivity is clearly demonstrated by the pulse arriving at the beginning of the fault-normal velocity time-series. It can be observed from Figure 1a that the peak ground velocity associated with the fault-normal component is larger in relation to the fault-parallel component. As a consequence, the fault-normal spectral acceleration (SA) amplitudes are also larger in the vicinity of the directivity pulse period (T_p = 7.2s, as determined using the pulse classification algorithm of Baker (2007)), as illustrated in Figure 1b.

The New Zealand (NZ) seismic design standard (NZS1170.5:2004) accounts for the effect of forward-directivity by means of a near-fault factor, which is based on the broadband directivity model of Somerville et al. (1997) and amplifies the elastic design response spectra over a wide range of vibration periods. In contrast, empirical evidence from previous earthquakes has consistently

demonstrated that the directivity pulse is 'narrowband' in nature, whose period increases with earthquake magnitude (M_w) (Somerville, 2003). As a result, the directivity amplification of spectral ordinates only occurs over a small/narrow range of periods surrounding the pulse period (refer to Figure 1b). The results of previous studies (e.g. Bradley, 2012a; Joshi, 2013) highlight that changes to the NZS1170.5:2004 near-fault factor are warranted. More importantly, these changes can be achieved by incorporating more appropriate narrowband directivity models in seismic hazard analyses which underpin design code response spectra as is demonstrated herein. This paper provides a summary of an extensive study carried out by Joshi (2013), to which readers are referred to for further detail.

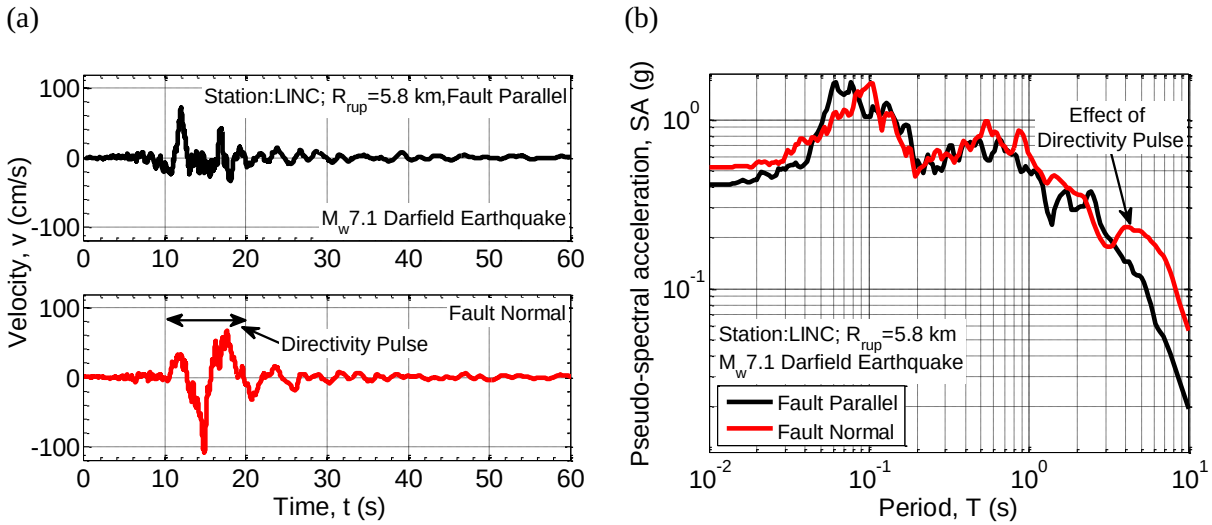

Figure 1:Evidence of strong forward-directivity effects in the: (a) fault-normal velocity time-series; and (b) pseudo-acceleration response spectrum observed at Lincoln (east of the Greendale fault) during the 4 September 2010 M_w7.1 Darfield earthquake.

2 INCORPORATION OF NEAR-FAULT DIRECTIVITY EFFECTS IN CONVENTIONAL PSHA

2.1 Directivity in ground motion prediction models

One output from PSHA is the annual rate of exceedance of a certain ground motion intensity measure, $\lambda(IM > im)$ at the site of interest (Kramer, 1996; McGuire, 2004). The analysis is conducted by combining: (i) all potential earthquake sources and their likelihood of occurrence (i.e. from the Earthquake Rupture Forecast (ERF)); and (ii) the distribution of ground motion produced by the earthquake sources should they occur (i.e. from an empirical ground motion prediction equation (GMPE)). Current empirical GMPEs do not make any provision for the aforementioned amplification of SA amplitudes caused by pulse-like ground motion features. The sole application of these GMPE models in conventional PSHA could therefore result in the underestimation of seismic hazard for a given near-fault site (Abrahamson, 2000; Shahi & Baker, 2011; Tothong et al., 2007). In this section, an approach to modify the predictions of GMPEs using the narrowband directivity model of Shahi & Baker (2011) (SB11) is described. The efficacy of this model for NZ has been validated by Joshi (2013) using observations from the Canterbury earthquakes. Equation (1) presents the functional form of the SB11 directivity model, which was calibrated empirically using pulse-like ground motions in the NGA (Next Generation Attenuation) database.

$$\mu_{lnAf|T_p} = \begin{matrix} 1.131 \exp\left(-3.11\left(\ln(T/T_p)+0.127\right)^2\right)+0.058 \ (\text{if } T \le 0.88\,T_p) \\ 0.924 \exp\left(-2.11\left(\ln(T/T_p)+0.127\right)^2\right)+0.255 \ (\text{if } T > 0.88\,T_p) \end{matrix} \quad (1)$$

where $\mu_{lnAf|T_p}$ represents the mean amplification factor for a given vibration period (T) and pulse period (T_p). Since the model is a function of T_p, which in turn is related to earthquake magnitude (M_w), and well-represented by a lognormal distribution (Shahi & Baker, 2011; Somerville, 2003), it is logical to employ a convolution integral to calculate the mean directivity amplification for a given M_w, as shown in Equation (2):

$$\mu_{\ln A_f} = \int \mu_{lnAf|T_p} f_{T_p} dT_p \quad (2)$$

where f_{T_p} denotes the distribution of the pulse period. The SB11 pulse period model is used on the basis of its improved predictive capabilities (Joshi, 2013) and is illustrated in Equation (3):

$$\ln(T_p) = -5.73 + 0.99M_w;\ \sigma_{\ln(T_p)} = 0.56 \quad (3)$$

where $\ln(T_p)$ and $\sigma_{\ln(T_p)}$ represent the median and standard deviation of the pulse period.

Given that pulse-like ground motions may not always be observed at sites located in the near-fault region (typically within source-to-site distances less than 20km), it is necessary to consider the probability of pulse occurrence. Using ground motion data from the latest NGA-West2 database, Shahi (2013) (S13) developed models for pulse probability from strike-slip and non-strike-slip events given by Equations (4) and (5), respectively:

$$P(pulse|R_{rup}, s, \theta) = \frac{1}{1+e^{0.7897+0.1378R_{rup}-0.3533\sqrt{s}+0.020\theta}} \quad (4)$$

$$P(pulse|R_{rup}, d, \phi) = \frac{1}{1+e^{1.483+0.1240R_{rup}-0.6880\sqrt{d}+0.022\phi}} \quad (5)$$

where, as shown in Figure 2, R_{rup} is the closest distance to the fault plane from the site; s and d relate to fault length for strike-slip and non-strike-slip events, respectively; and θ and ϕ relate to difference in angles between the rupture direction and the site from the hypocentre.

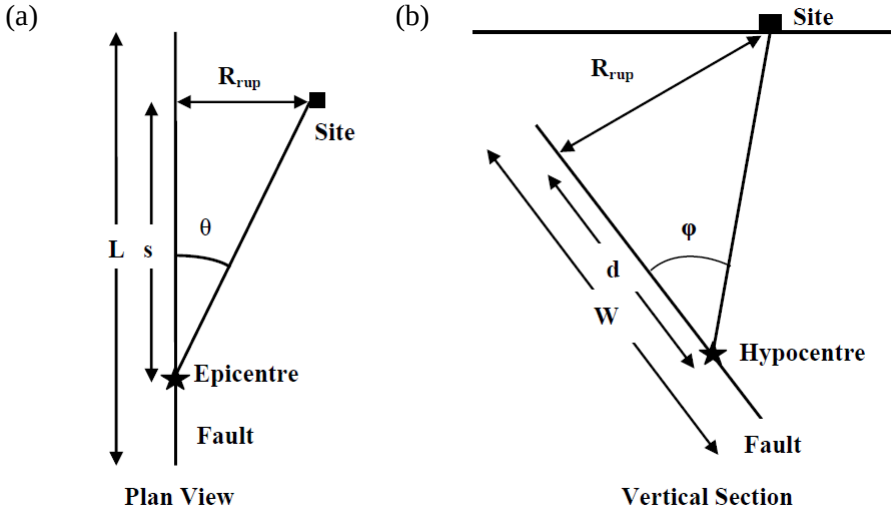

Figure 2: Source-to-site geometry illustrating the parameters used in the development of empirical pulse probability models for: (a) strike-slip; and (b) non strike-slip faults (modified from Somerville et al, 1997).

Based on the above information, it is possible to evaluate the directivity-corrected SA amplitudes (SA_{dir}) for the earthquake rupture scenario and vibration period of interest (T), as shown in Equation (6):

$$SA_{dir}(T) = SA(T) \cdot \exp\left(\mu_{\ln A_f}\right) \cdot P(Pulse) + SA(T) \cdot \exp\left(\mu_{ln\,D_f}\right) \cdot [1 - P(Pulse)] \quad (6)$$

where $SA(T)$ represents the median GMPE prediction (for a given rupture, Rup_i) of the horizontal geometric mean SA; $P(Pulse)$ is the predicted pulse probability; and $\mu_{ln\,D_f}$ represents a deamplification factor to account for the possibility of observing non-pulse-like ground motions at the site of interest (refer to Shahi & Baker (2011) for further details). A reduction factor (R_f) for the lognormal standard deviation associated with the GMPE (σ_{lnSA}) is also prescribed by the SB11 model, and accounts for the reduction in uncertainty of the predictions as a result of accounting for the effects of pulse-like ground motions. It is noted that the reduction factor can be applied in a manner similar to Equation (6) and its functional form is suppressed herein for brevity.

An example application of the NZ-specific Bradley (2010; 2013) GMPE with and without considering the effects of near-fault directivity is illustrated in Figure 3 for a M_w7.0 strike-slip fault (with a length of 43km based on the Wells & Coppersmith (1994) magnitude-scaling relation). Figure 3a, in particular, illustrates the predicted SA amplitudes for the case where the location of the epicentre (or hypocentre) is varied while keeping the site location constant (i.e. varying rupture length, s and constant source-to-site azimuth, θ). As expected, increasing levels of amplification are predicted by the SB11 model for larger s values in the vicinity of the pulse period (T_p = 3.3 s). For the case where the location of the epicentre and site coincide (s = 0), the model predicts a de-amplification of spectral ordinates to account for the low possibility of observing pulse-like ground motions. In addition, the narrowband nature of the model is most clearly visible when a scenario-based approach is used to apply the model i.e. by assuming the occurrence of a pulse at the site (P_{pulse} = 1). Similarly, Figure 3b considers the case where the hypocentre location is kept constant and the site distance perpendicular to the fault is varied (i.e. constant rupture length, s and varying source-to-site azimuth, θ). It is evident from the source-to-site geometry in Figure 2a that as R_{rup} increases, so does θ. This has two important implications as shown in Figure 3b: (i) there is a systematic reduction in spectral amplitudes predicted by the B10 GMPE due to the effects of geometric spreading and anelastic attenuation; and (ii) the level of directivity amplification predicted by the SB11 model decreases due to a reduction in the predicted probability of pulse occurrence. It can be seen that at a distance of 30km (θ = 45°), the effect of directivity is essentially negligible.

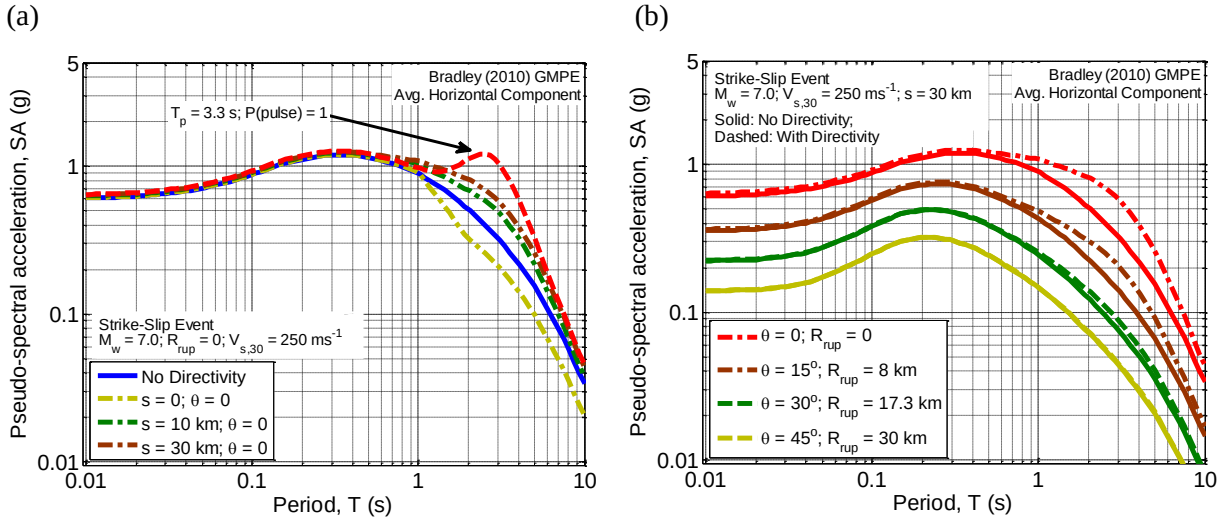

Figure 3: Illustration of the narrowband directivity model of Shahi & Baker (2011) on the predicted response spectra obtained using the Bradley (2010; 2013) GMPE for a M_w7.0 strike-slip earthquake: (a) predicted response spectra for a site located in the direction of rupture propagation but with varying epicentre locations; and (b) predicted response spectra for sites located at increasing source-to-site distances but with the epicentre location held constant. Note that the predictions are also shown without correcting for directivity in both cases.

It is worth noting that frameworks to incorporate the directivity phenomenon in seismic hazard calculations have been proposed in previous research. In fact, its importance was first highlighted by Abrahamson (2000) who used a modified version of the Somerville et al. (1997) broadband model to quantify directivity effects on the geometric mean and fault-normal components of SA. More recently, Shahi & Baker (2011) considered the effects of pulse-like ground motions in PSHA by extending a framework initially proposed by Tothong et al. (2007) and Iervolino & Cornell (2008). In essence, this approach involves sub-dividing the mean annual rate of exceeding a certain level of SA into near-fault ($\lambda(SA > sa)_{NF}$) and far-fault ($\lambda(SA > sa)_{FF}$) terms. While $\lambda(SA > sa)_{FF}$ can be estimated using conventional PSHA, $\lambda(SA > sa)_{NF}$ requires the use of empirical models to predict: (i) the probability of pulse occurrence; and (ii) the effect of pulse-like ground motions on SA amplitudes obtained from GMPEs. Although the models developed by Shahi & Baker (2011) are used herein, the proposed approach in this paper does not require $\lambda(SA > sa)$ to be separated into distinct near- and far-fault terms.

2.2 **Consideration of distributed seismicity as finite-fault sources**

The possibility of earthquake occurrence on unknown faults is accounted for in the NZ ERF (Stirling et al. 2002; Stirling et al., 2012) by the use of distributed seismicity. In Stirling et al. (2002, 2012), distributed seismicity is modelled as point-sources located at depths ranging between 10km and 90km. As illustrated by Bradley (2012a), this point-source representation can result in unconservative estimates of the predicted surface ground motion in seismic hazard calculations. In the present study distributed seismicity point-sources in the NZ ERF are represented as equivalent finite-faults using the: (i) point-source location and its associated strike, dip and rake angles; (ii) moment magnitude (M_w) obtained from the Gutenberg-Richter (G-R) distribution assigned to each point-source; and (iii) magnitude scaling relations of Wells & Coppersmith (1994) to define the fault geometry (refer to Joshi (2013) for further information).

3 **EXAMPLES OF NZ-SPECIFIC PSHA INCLUDING DIRECTIVITY**

This section summarises the results associated with the application of the previously described procedure to NZ-specific PSHA. Generic locations in Christchurch (latitude: -43.5300°; longitude: 172.6300°; site class D: deep soil) and Otira (latitude: -42.8302°; longitude: 171.5647°; site class B: weak rock) are selected based on differences in the major contributing sources of seismicity to the overall seismic hazard. At the 475-year return period, distributed seismicity sources provide a significant contribution to Christchurch's hazard, whereas, Otira's hazard is dominated by major fault sources (Alpine, Kelly and Hope faults). An exposure period of 50 years is adopted for all seismic hazard analyses whose results are presented herein. In addition, the latest NZ ERF (Stirling et al., 2012) and Bradley (2010; 2013) GMPE are used to carry out the analyses. From the example application in Figure 3, it is evident that the hypocentre location on the causative fault must be defined in order to account for directivity effects in PSHA. For the purposes of computational efficiency, it was considered reasonable to define hypocentres at three evenly distributed locations along-strike. Based on the results of an extensive statistical study carried out by Mai et al. (2005), the hypocentre location was located 60% of the fault width in the down-dip direction.

3.1 **Effect of finite-fault representation for distributed seismicity**

Before scrutinising the effect of directivity in PSHA, it is important to firstly quantify the effects of using point-source and finite-fault based representations of the distributed earthquake sources since directivity cannot be considered for point sources. Attention here is restricted to the site in Christchurch due to the significance of background seismicity for the region. Figures 4a and 4c illustrate the seismic hazard curves for peak ground acceleration (PGA) and SA(3s). The hazard curves have been obtained considering only distributed seismicity sources, which are defined as: (i) point-sources (i.e. as defined in the NZ ERF); (ii) finite-faults with dimensions that are consistent with the M_w of each possible event in the source's G-R distribution (i.e. 'exact' representation); and (iii) finite faults with dimensions corresponding to the maximum magnitude (M_{max}) from the G-R distribution associated with each point-source. The latter form of representation was considered for reasons which will become apparent in the discussion to follow. Also shown in Figure 4 is an 'error ratio', which is defined as the ratio of the intensity measure obtained using methods (i) and (iii) normalised by the value obtained using the 'exact' approach for each exceedance probability (PE). An error ratio less than 1 indicates under-estimation whereas a ratio greater than 1 implies over-estimation of the seismic hazard.

As expected, the results of Figure 4 illustrate that the point-source representation of distributed earthquakes results in an under-estimation of both IMs at 10% and 2% in 50-year PEs. In particular, the error ratios indicate that the under-estimation ranges between 5-10% and 10-15% for the two PEs, respectively. However, for the 50% in 50-year PE, there is negligible error. The importance of using the 'exact' geometry in defining the finite-faults is clearly illustrated by the hazard curves and error ratios corresponding to the maximum M_w fault representation of each point-source. For the 10% and 2% in 50-year PEs, it can be observed that using the latter approach results in an over-estimation of the hazard for both IMs. Specifically, the level of over-estimation ranges between 15-35% (10% in 50-year PE) and 15-40% (2% in 50-year PE), with the lower and upper limits of these ranges

corresponding to the PGA and SA(3s), respectively. This can be attributed to smaller source-to-site distances (R_{rup}) obtained using the larger fault geometry associated with the maximum M_w for each distributed seismicity source. Similarly, in the case of the 50% in 50-year PE, the hazard over-estimation is only notable for long period ground motion (i.e. SA(3s)).

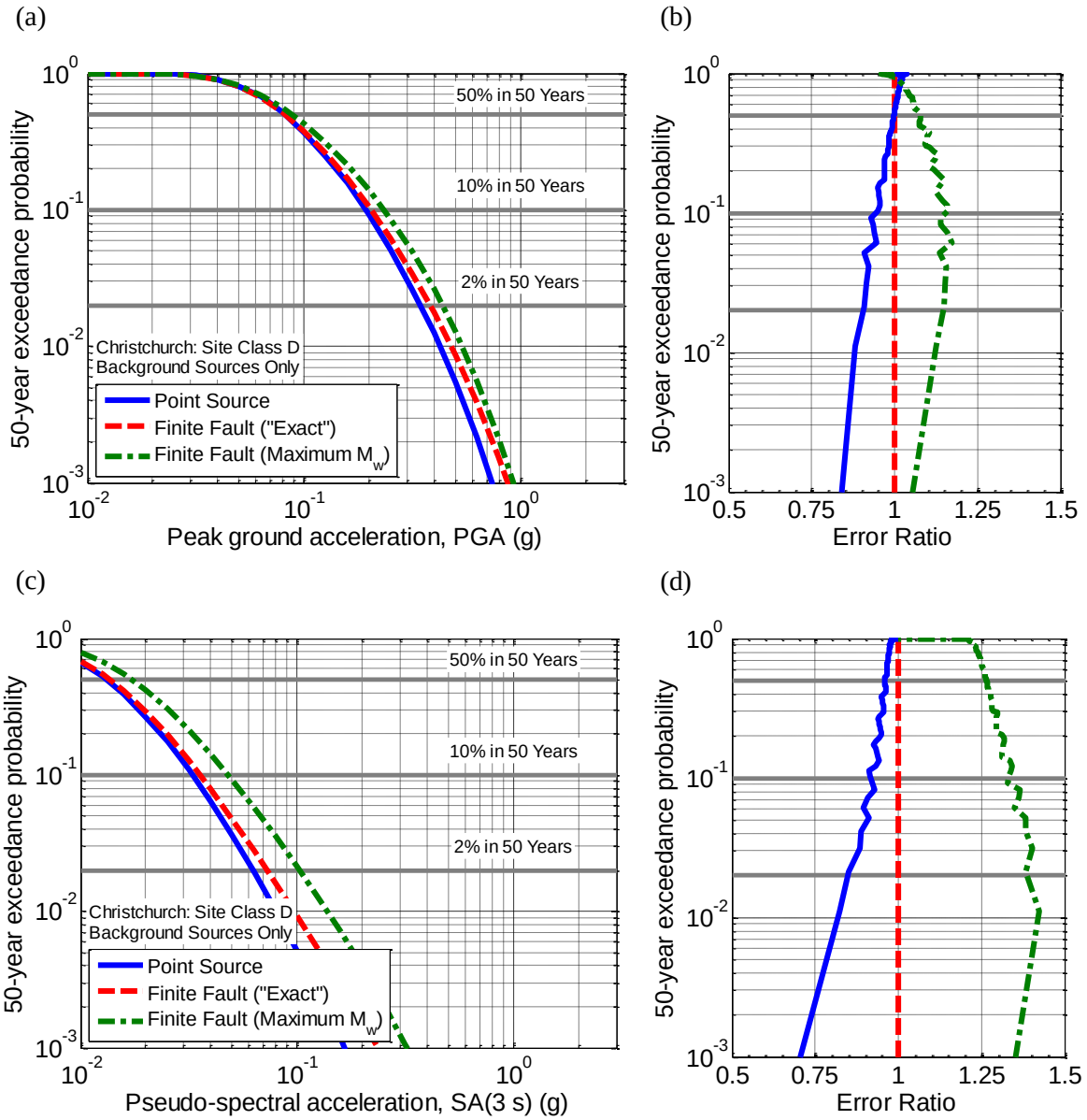

Figure 4: Importance of characterising distributed earthquake sources using the 'exact' finite-fault geometry illustrated by means of seismic hazard curves calculated for a site in Christchurch (for PGA and SA(3s)).

3.2 **Effect of directivity consideration**

In order to quantify the effect of near-fault directivity for Christchurch and Otira, seismic hazard analyses were conducted for $0.01\text{s} \leq T \leq 10\text{s}$ using the approach outlined in the previous section. For the purposes of comparison, the analyses were repeated using both point-source and 'exact' finite-fault representations of the distributed seismicity sources. It is worth re-iterating that in the former case, directivity effects cannot be considered (because of an absence of fault geometry). Figure 5 illustrates: (i) uniform hazard spectra (UHS) corresponding to the 10% in 50-year PE, with and without accounting for directivity effects; and (ii) a 'hazard ratio' defined as the ratio of all UHS normalised by the base case i.e. UHS considering fault and background point-sources without directivity for both locations. Based on the results of Figures 5a and 5c, it can be concluded that, at the 10% in 50-year PE, directivity effects are not significant for Christchurch. In particular, the contribution of fault

sources to the directivity amplification is negligible (because such sources are not near Christchurch). This statement can be validated by the hazard ratio, which effectively remains unchanged at all periods after accounting for directivity using fault sources only (i.e. since the calculation of directivity amplification is not possible for distributed point-sources). Upon considering the distributed seismicity as finite-faults, it can be observed that there is an increase in the hazard ratio of up to 5%. Although not shown here, the hazard ratio progressively increases with decreasing exceedance probabilities. Upon correcting for directivity, there is a slight reduction in the hazard ratio at periods less that T = 0.4s. This can be attributed to deamplification of spectral ordinates predicted by the SB11 model to account for the occurrence of non-pulse-like ground motions, as described previously. For Christchurch, amplification due to directivity occurs in the period range 0.7s $\leq T \leq$ 3s, and is especially notable at the 2% in 50-year PE (refer to Joshi (2013) for further details). For example, the largest increase in the 2% in 50-year PE (8%) is approximately twice that of the 10% in 50-year PE (4%). The low levels of amplification can be attributed to the low probabilities of pulse occurrence predicted by the S13 model for the distributed fault sources. This is consistent with the fact that the distributed seismicity for Christchurch is dominated by reverse faults and that the S13 model always predicts smaller pulse probabilities for non strike-slip faults due to reasons mentioned in Joshi (2013). The consideration of background seismicity in the Canterbury region as exclusively reverse faulting events is presumably a conservative assumption, since such events produce on average larger ground shaking than strike-slip events. However, the above point potentially implies that this is in fact unconservative at long periods, where strike-slip events give a notably larger probability of directivity.

In contrast, Figures 5b and 5d highlight the fact that near-fault directivity effects are significant for the Otira site at vibration periods greater than T = 2s. It is important to note that the UHS represents an envelope of spectral ordinates resulting from a combination of ground motions with different magnitudes, distances and pulse periods. As a result, the narrowband nature of the amplification predicted by the SB11 model is somewhat masked in Figure 5b. This observation is consistent with the findings of previous researchers including Shahi & Baker (2011) and Chioccarelli & Iervolino (2012). Because the hazard is dominated by fault sources at all vibration periods, it can be seen from the hazard ratio that the effect of considering directivity for the distributed seismicity sources is negligible (a trend observed for all exceedance probabilities). The significant directivity amplification for Otira can be attributed to higher pulse probabilities predicted by the S13 model due to the proximity and strike-slip faulting mechanism of the aforementioned fault sources which control the seismic hazard. In the Christchurch example, the amplification became notable for the 2% in 50-year PE. However, for the Otira site, the increase in hazard is similar for the two exceedance probabilities. For example, the largest increase in hazard is 34% for the 10% in 50-year PE (Figure 5b) and 32% for the 2% in 50-year PE (Joshi, 2013), both of which occur at T = 5s.

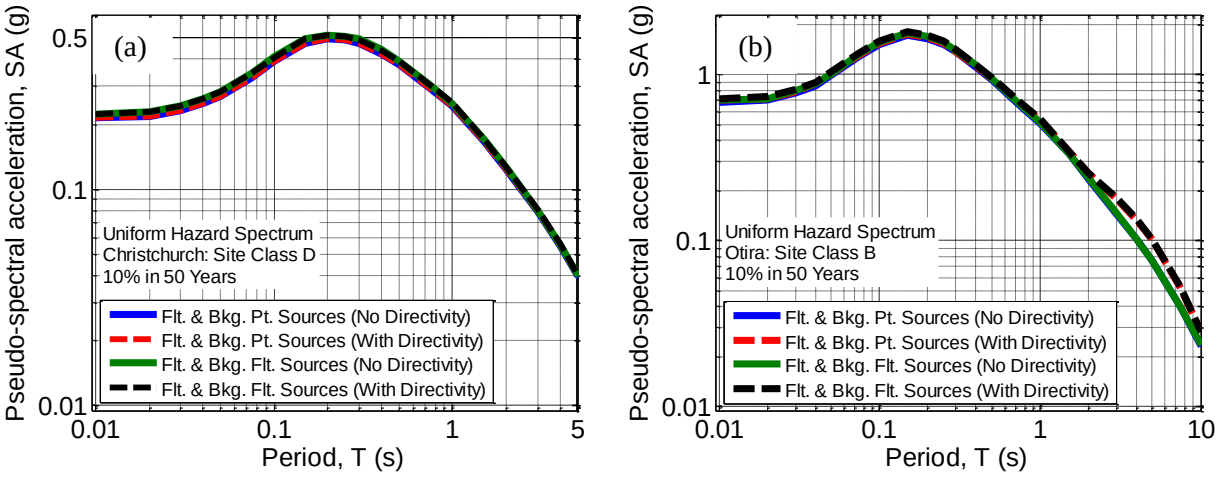

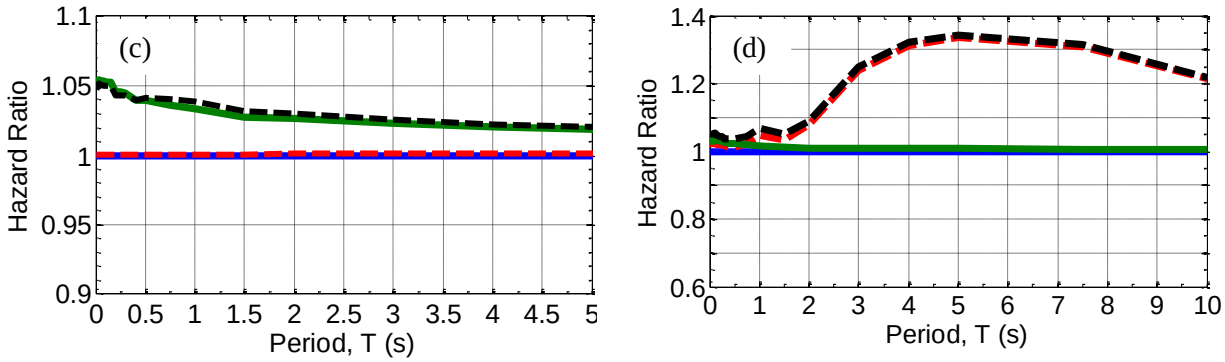

Figure 5: UHS calculated with and without considering the effects of near-fault directivity at an exceedance probability of 10% in 50 years for typical sites in: (a) Christchurch; and (b) Otira. The bottom panels illustrate a 'hazard' ratio which indicates the increase/decrease in hazard as a result of consdering directivity effects.

Another useful exercise is to link the predominant sources obtained from deaggregation corresponding to periods at which the largest directivity amplification is observed. For the location in Christchurch, it is appropriate to consider the deaggregation of hazard for SA(1s) at the 2% in 50-year PE (refer to Figure 6a) based on the period range (i.e. 0.7s $\leq T \leq$ 3s) over which the amplification was observed. It is evident that the hazard is controlled by: (i) small-to-moderate magnitude earthquakes (M_w < 7.0) on distributed fault sources at relatively short distances (R_{rup} $\leq$ 50km); and (ii) large magnitude earthquakes on the Alpine Fault (M_w8.1, R_{rup} = 133km), Porter's Pass Fault (M_w7.5, R_{rup} = 44km), Pegasus Fault (M_w7.0, R_{rup} = 22km) and Ashley Fault (M_w7.2, R_{rup} = 31km). It was identified previously that the fault sources produce marginal levels of directivity amplification based on the low pulse probabilities resulting from the large source-to-site distances. Hence, it was deduced that the observed amplification is caused mainly by the distributed fault sources. This is not reflected by the mean magnitude ($M_{w,mean}$ = 6.9) and distance ($R_{rup,mean}$ = 46.4km) from the deaggregation of hazard for SA(1s), which is likely due to a skewing effect caused by the fault sources. Although not shown here, the deaggregation of hazard considering only distributed fault sources provides a mean magnitude and distance of 6.5 and 27.6km, respectively. Based on the empirical model of Shahi & Baker (2011) illustrated in Equation (3), this corresponds to a median pulse period of 1.9s, which falls within the aforementioned period range corresponding to directivity amplification.

Given that the maximum directivity amplification for Otira was observed at T = 5s, it is logical to expect that the pulse period associated with the mean earthquake magnitude from the deaggregation for SA(5s) would also be similar. The importance of fault-based seismicity in the region is clearly illustrated by the deaggregation plot for SA(5s) corresponding to the 2% in 50-year PE in Figure 6b. In particular, the seismic hazard is dominated by the Kelly Fault, which is capable of producing M_w7.3 earthquakes and is located at a distance of R_{rup} = 1.5km from the site. This is followed by significantly smaller contributions from the Browning (M_w6.9, R_{rup} = 4.6km) and Alpine faults (M_w8.1, R_{rup} = 11.7km). The median pulse period predicted by the SB11 model for the mean M_w of 7.3, is equal to T_p = 4.6s, which is in the period range corresponding to the maximum directivity amplification observed previously in Figure 5b.

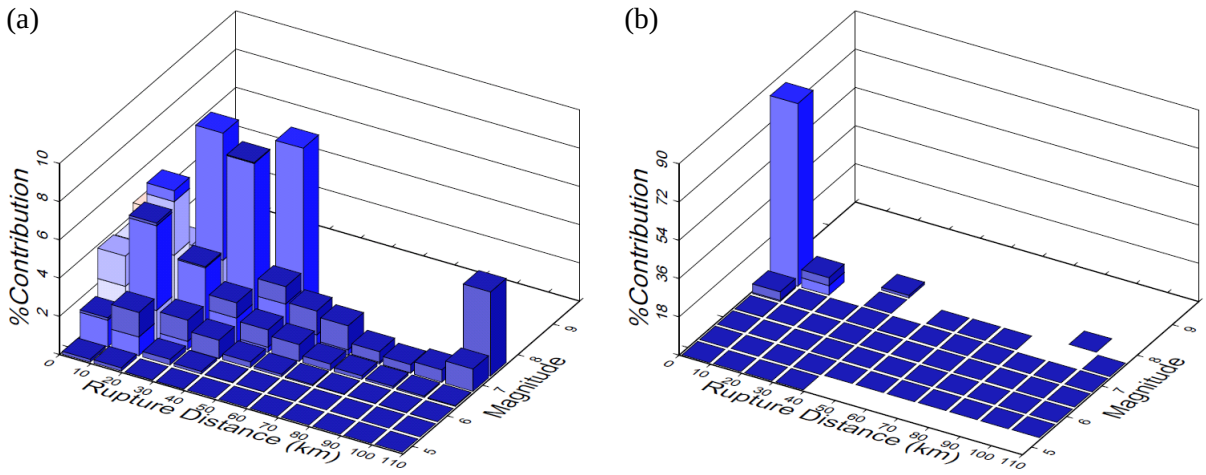

Figure 6: Seismic hazard deaggregation for typical sites in: (a) Christchurch (SA(1s)); and (b) Otira (SA(5s)) at an exceedance probability of 2% in 50 years. Note that the hazard calculations are performed considering directivity effects and treating distributed earthquake sources as finite-faults.

4 COMPARISON WITH NZS1170.5:2004 GUIDELINES FOR NEAR-FAULT DIRECTIVITY EFFECTS

In this section, a comparison between the directivity amplification obtained from NZ-specific PSHA and the NZS1170.5:2004 prescription using the near-fault factor, N, is carried out. It is worth noting that NZS1170.5:2004 is based on the results of seismic hazard analyses carried out using the McVerry et al. (2006) GMPE, which predicts the 'larger' component of SA i.e. the larger value of SA (for a given period, T) obtained from two as-recorded orthogonal components of ground motion. On the other hand, the seismic hazard analyses carried out in the previous section used the Bradley (2010) GMPE, which predicts the geometric mean of SA obtained from two as-recorded orthogonal components of ground motion. Therefore, prior to carrying out the aforementioned comparison, it is important to convert the directivity amplification obtained from PSHA to the 'larger' component using ground motion directionality ratios (refer to Joshi (2013) for further details).

Figures 7a and 7b provide a comparison between the converted directivity amplification for Christchurch and Otira (corresponding to the 10% and 2% in 50-year *PE*s) with the near-fault factor, respectively. It is noted that the maximum permissible increase allowed by NZS1170.5:2004 for the near-fault factor is used herein. For Christchurch, it can be observed that for T < 2.5s, the observed amplification exceeds the code-based prescription by up to approximately 40% for both exceedance probabilities. At longer periods, the trend is reversed, with the increase in hazard defined by the near-fault factor being up to 26% greater than the PSHA amplification in each case. In reality, it should be noted that the near-fault factor is not applied for the seismic design of structures in Christchurch because it is not located within 20km of any major faults (Standards New Zealand, 2004). Hence, it is likely that the current design guidelines for the Christchurch region do not adequately account for the effects of near-fault directivity.

For the location in Otira, it is evident from Figure 7b that the NZS1170.5:2004 near-fault factor amplification is lower than the PSHA directivity amplification associated with both *PE*s for a majority of vibration periods (i.e. T < 7s). Similar to the previous example, the largest under-prediction in this case is as high as 40%. Although not considered herein, the results of this section indicate that similar trends are likely to be observed for Wellington, where the seismic hazard is dominated by both subduction interface and active shallow crustal sources. More importantly, the above comparisons allude to the fact that a revision to the near-fault factor is warranted in the development of a future seismic design standard for NZ. In addition, the narrowband nature of the directivity pulse is not captured by the Somerville et al. (1997) model, which forms the basis of the code-based directivity prescription, as mentioned previously.

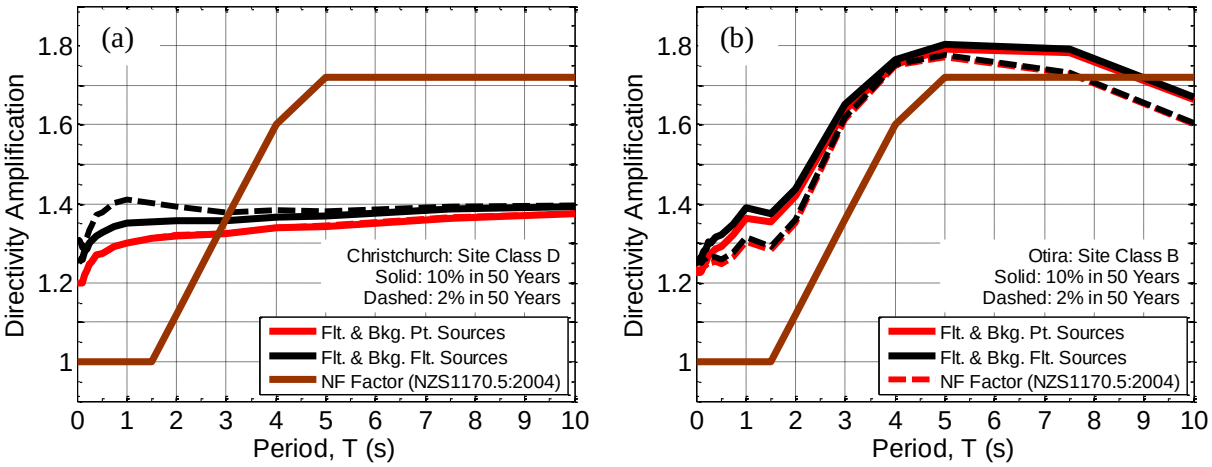

Figure 7: Comparison of the directivity amplification obtained from PSHA for typical locations in: (a) Christchurch; and (b) Otira with the near-fault factor from NZS1170.5:2004.

5 CONCLUSIONS

This paper has focused on explicitly incorporating the effects of near-fault directivity in NZ-specific PSHA using recently developed empirical models by Shahi & Baker (2011). The models account for both the 'narrowband' nature of the directivity pulse on spectral ordinates and probability of pulse occurrence at the site of interest. Based on the findings of a recent study by Bradley (2012a), it was deemed necessary to consider the distributed/background seismicity as finite-fault sources, as opposed to their conventional treatment as point-sources. This also allowed the directivity phenomenon to be considered appropriately for background earthquakes.

The significance (or lack thereof) of explicit inclusion of directivity in PSHA was illustrated for the entire vibration period range ($0.01\text{s} \leq T \leq 10\text{s}$) at typical sites located in Christchurch and Otira, two locations whose seismic hazard is comprised of notably different seismic sources. It was illustrated that using the 'exact' finite-fault representation of the background sources results in improved estimates of the hazard, with larger ground motion intensities being predicted at longer periods. For example, in Christchurch (where background sources provide a significant contribution to the total hazard), the increase in the 2475-year return period hazard for PGA and $SA(3\text{s})$ was approximately 10% and 15%, respectively. Based on the results of PSHA, it was found that the maximum increase in hazard due to directivity effects is less than 10% for Christchurch at the 2% in 50-year PE, and occurred in the period range, $0.7\text{s} \leq T \leq 3\text{s}$. At higher exceedance probabilities, the observed increase was either marginal or non-existent. The low levels of amplification were attributed to (i) large source-to-site distances of fault sources; (ii) small-to-moderate magnitudes of the contributing background earthquakes; and (iii) relatively low pulse probabilities assigned to the background sources as a result of their reverse faulting-mechanism. In contrast, notable directivity amplification (15-35% increase in hazard for periods greater than 2s at exceedance probabilities of 10% and 2% in 50 years) was observed at Otira. This was consistent with the proximity of the site to major sources of seismicity including the strike-slip Kelly, Browning and Alpine faults. Comparisons of the observed amplification at both sites with the near-fault factor indicated that the NZS1170.5:2004 prescription for near-fault effects is generally inadequate for a large range of vibration periods. More importantly, based on the methodology outlined in this paper, directivity effects could be directly incorporated in seismic hazard analyses underpinning design codes – thus removing the need for a ‘near-fault’ factor.

REFERENCES

Abrahamson, N. A. (2000). Effects of rupture directivity on probabilistic seismic hazard analysis. In *Proceedings of the 6th International Conference on Seismic Zonation*. Palm Springs, California.

Baker, J. W. (2007). Quantitative classification of near-fault ground motions using wavelet analysis. *Bulletin of the Seismological Society of America*, *97*(5), 1486–1501. doi:10.1785/0120060255

Bradley, B. A. (2012a). *Ground Motion and Seismicity Aspects of the 4 September 2010 and 22 February 2011 Christchurch Earthquakes* (Technical report prepared for the Canterbury Royal Commission) (p. 62). Department of Civil and Natural Resources Engineering, University of Canterbury.

Bradley, B. A. (2012b). Strong ground motion characteristics observed in the 4 September 2010 Darfield, New Zealand earthquake. *Soil Dynamics and Earthquake Engineering*, *42*, 32–46. doi:10.1016/j.soildyn.2012.06.004

Bradley, B. A. (2013). A New Zealand-Specific Pseudospectral Acceleration Ground-Motion Prediction Equation for Active Shallow Crustal Earthquakes Based on Foreign Models. *Bulletin of the Seismological Society of America*, *103*(3), 1801–1822. doi:10.1785/0120120021

Bradley, B. A., & Cubrinovski, M. (2011). Near-source Strong Ground Motions Observed in the 22 February 2011 Christchurch Earthquake. *Seismological Research Letters*, *82*(6), 853–865. doi:10.1785/gssrl.82.6.853

Bradley, Brendon A. (2010). *NZ-Specific Pseudo-Spectral Acceleration Ground Motion Prediction Equations Based on Foreign Models* (Research Report No. 2010-03) (p. 316). Department of Civil and Natural Resources, University of Canterbury.

Chioccarelli, E., & Iervolino, I. (2012). Near-source seismic hazard and design scenarios. *Earthquake Engineering & Structural Dynamics*, n/a–n/a. doi:10.1002/eqe.2232

Iervolino, I., & Cornell, C. A. (2008). Probability of occurrence of velocity pulses in near-source ground motions. *Bulletin of the Seismological Society of America*, *98*(5), 2262–2277. doi:10.1785/0120080033

Joshi, V. A. (2013). *Near-Fault Forward-Directivity Aspects of Strong Ground Motions in the 2010-11 Canterbury Earthquakes* (Master of Engineering Thesis). University of Canterbury, Christchurch, New Zealand.

Joshi, V. A., & Bradley, B. A. (2013). Empirical Analysis of Near-Fault Forward-Directivity Effects in the Canterbury Earthquakes (p. 11pp). Presented at the New Zealand Society for Earthquake Engineering Conference, Wellington, New Zealand.

Kramer, S. L. (1996). *Geotechnical Earthquake Engineering*. Upper Sadle River, New Jersey: Prentice Hall.

McGuire, R. K. (2004). *Seismic Hazard and Risk Analysis*. Berkeley, California: Earthquake Engineering Research Institute.

McVerry, G. H., Zhao, J. X., Abrahamson, N. A., & Somerville, P. G. . (2006). New Zealand acceleration response spectrum attenuation relations for crustal and subduction zone earthquakes. *Bulletin of the New Zealand Society for Earthquake Engineering*, *39*(4), 1–58.

Shahi, S. K., & Baker, J. W. (2011). An empirically calibrated framework for including the effects of near-fault directivity in probabilistic seismic hazard analysis. *Bulletin of the Seismological Society of America*, *101*(2), 742–755. doi:10.1785/0120100090

Somerville, P. G. (2003). Magnitude scaling of the near fault rupture directivity pulse. *Physics of the Earth and Planetary Interiors*, *137*(1-4), 201–212. doi:10.1016/S0031-9201(03)00015-3

Somerville, P. G., Smith, N. F., Graves, R. W., & Abrahamson, N. A. (1997). Modification of empirical strong ground motion attenuation relations to include the amplitude and duration effects of rupture directivity. *Seismological Research Letters*, *68*(1), 199–222.

Standards New Zealand. (2004). *NZS1170.5:2004, Structural Design Actions, Part 5: Earthquake actions- New Zealand*. Wellington, New Zealand.

Stirling, M., McVerry, G., Gerstenberger, M., Litchfield, N., Van Dissen, R., Berryman, K., … Jacobs, K. (2012). National Seismic Hazard Model for New Zealand: 2010 Update. *Bulletin of the Seismological Society of America*, *102*(4), 1514–1542. doi:10.1785/0120110170

Stirling, M. W., Mc Verry, G. H., & Berryman, K. R. (2002). A new seismic hazard model for New Zealand. *Bulletin of the Seismological Society of America*, *92*(5), 1878–1903.

Tothong, P., Cornell, C. A., & Baker, J. W. (2007). Explicit directivity-pulse inclusion in probabilistic seismic hazard analysis. *Earthquake Spectra*, *23*(4), 867–891. doi:10.1193/1.2790487

Wells, D. L., & Coppersmith, K. J. (1994). New empirical relationships among magnitude, rupture length, rupture width, rupture area, and surface displacement. *Bulletin of the Seismological Society of America*, *84*(4), 974–1002.